### **ORIGINAL PAPER**



# Exploring the molecular solvatochromism, stability, reactivity, and non-linear optical response of resveratrol

Igo T. Lima<sup>1</sup> · Ramon F. C. Gomes<sup>1</sup> · Edson N. C. Paura<sup>2</sup> · Patricio F. Provasi<sup>3</sup> · Rodrigo Gester<sup>4,5</sup> · Antonio Rodrigues da Cunha<sup>2</sup>

Received: 14 March 2024 / Accepted: 8 August 2024 / Published online: 21 August 2024 © The Author(s), under exclusive licence to Springer-Verlag GmbH Germany, part of Springer Nature 2024

#### **Abstract**

Context This work analyzes the isomerization effects and solvent contributions to the stability, electronic excitations, reactivity, and non-linear optical properties (NLO) of resveratrol molecules within the formalism of the Density Functional Theory. The findings suggest that resveratrol solvatochromism is significantly influenced by solvent polarization. The electronic and free energies (E and G) indicate that *trans* is the most stable conformer. The system is classified as a strong nucleophile. However, the analysis of the Fukui functions and the Mulliken charges indicate that *cis-trans* isomerization jointly affects the reactive indices of the carbon and hydrogen atoms. The results also suggest that solvent is relevant to solvatochromism and the NLO response. Both *cis* and *trans* conformers present strong  $\pi - \pi^*$  excitations that undergo a visible hypsochromic change when the polarity of the solvent increases. Once the absorption spectra are connected to the first hyperpolarization ( $\beta$ ) by the Oudar and Chemla relation, the hypsochromism of resveratrol is the reason for the drop in the generation of the second harmonic when the ambient polarity decreases. The CAM-B3LYP DFT results suggest that resveratrol is interesting for NLO applications. Depending on the choice of solvent, values  $\sim 50$  times those observed for urea ( $\beta = 0.34 \times 10^{-34}$  esu), which is a standard NLO material.

**Methods** The optimized geometries of *cis* and *trans* isomers of resveratrol in vacuum were obtained using Density Functional Theory (DFT) with the hybrid exchange-correlation function (CAM-B3LYP) and Pople basis set functions, specifically 6-311++G(d,p). The solvent effect on the geometries of both isomers was included using the polarizable continuum model (PCM) with the same level of QM calculation. Vibrational analysis was conducted to confirm that all optimized geometries correspond to the minimum energy. Various electronic properties, including dipole moments, molecular orbitals, transition energy, dipole polarizabilities, and global reactivity parameters, were calculated using both continuum and discrete solvation models based on the sequential QM/MM methodology. All QM calculations were performed with the Gaussian 09 program and the MC simulations with the DICE program. All NLO analysis was carried out using the Multiwfn code.

Keywords Thermochemistry · UV-Vis spectra · Reactivity · NLO response · DFT · Solvent effects

#### Introduction

Two reasons can be mentioned regarding the liquid phase model. First, the environment can easily affect any molecular property. Furthermore, all chemical reactions relevant to biological and chemical processes occur in solution. Among these effects, solvatochromism observed in atoms and molecules is the best-known effect attributed to the solvent. In this case, specific solute-solvent interactions can affect the shape, intensity, and position of the electron absorption and emission spectra [1], which opens a path for various

optical applications. For example, recognition of emission and absorption electronic excitations and know-how to tune these spectral lines are essential to propose applications such as biological probes and sensors [2, 3].

Several reasons make some stilbene derivatives, such as resveratrol (3,5,4'-trihydroxystilbene, Fig. 1), an interesting study case. From the structural point of view, these chromophores can exist under cis-(Z) or trans-(E) structures and present two aromatic rings that can be functionalized with different electron donor (D) or acceptor (A) terminals. Furthermore, these rings are permanently linked by an ethylene moiety (HC=CH), constituting a complete push-pull D- $\pi$ -A system. In both isomers of resveratrol, the beta group acts





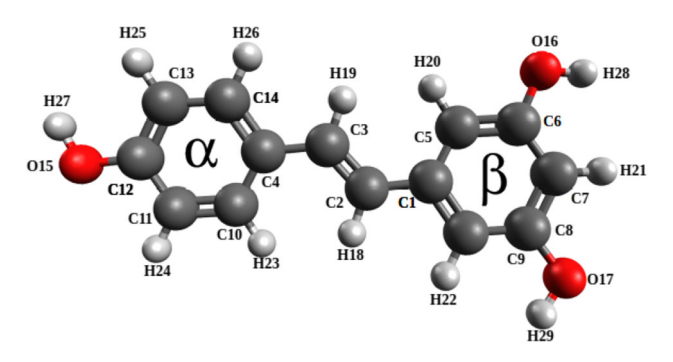


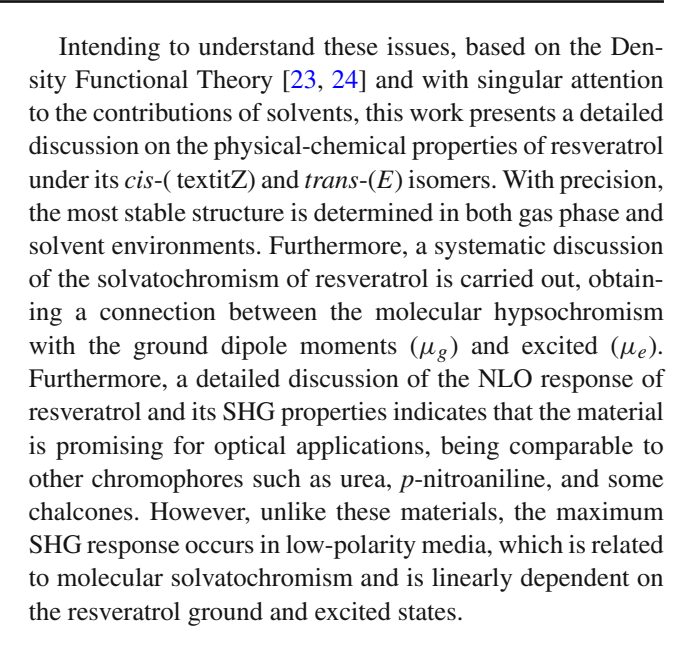
**Fig. 1** Geometry structure and atomic numbering of Resveratrol in its *trans* isomer form. The torsions  $\Phi_1$  and  $\Phi_2$  referred in the text are defined by the atoms 10-4-3-2, and 5-1-2-3, respectively

as the electron donor, while the alpha group serves as the electron acceptor, as previously indicated [4, 5].

Strong effects on NLO properties have been associated with D- $\pi$ -A systems. The second harmonic generation (SHG) is particularly significant among these effects. This effect is related to the two-photon absorption process. It is mainly dominated by the magnitude of the first hyperpolarizability ( $\beta$ ) but also depends on the molecular dipole moment ( $\mu$ ), which is strongly affected by various effects such as solute-solvent interactions [6], and molecular isomerization [7], for example.

Typically, chromophores with push-pull characteristics would be the focus of various physicochemical attacks. However, as resveratrol has recognized antioxidant properties, most discussions have been restricted to biological applications such as antitumor, antioxidant, antiviral, phytoestrogen, and significant cytotoxic effects when used at higher concentrations [8–11]. It is important to note that previous studies have shown that the trans-isomer exhibits higher biological activity and stability than the *cis*-isomer [12–14]. The trans-isomer has shown potential superiority across various biological contexts, including antitumor, antioxidant, and antiviral properties [15–18]

The resveratrol-light interaction is a curious phenomenon that attracts attention and may have many implications. When the polarity of the environment increases, bathochromic behavior is expected, which essentially is a shift of the electronic spectra toward lower energies. However, some reports indicate that resveratrol and its derivatives pre-establish the opposite and rare hypochromic effect around  $\sim 20$  nm [19, 20]. Furthermore, regardless of stability, high-frequency light can activate and alternate the *cis* and *trans* structures, giving rise to an NLO effect known as photoinduced birefringence, which dramatically affects the refractive index [21, 22]. Despite the relevance of such topics, no discussion comes close to discussing and addressing resveratrol hypsochromism or its effects on the NLO response.



# **Materials and methods**

The *cis* and *trans* isomers of resveratrol were subjected to geometric optimization and vibrational frequency calculation in gas using quantum mechanics (QM). Various electronic properties, including dipole moments, molecular orbitals, transition energy, dipole polarizabilities, and global reactivity parameters, were determined using density functional theory (DFT) [25]. The calculations employ the hybrid exchange-correlation function (CAM-B3LYP) [26] and Pople basis set functions, specifically 6-311++G(d,p) [27]. This DFT functional has successfully predicted the molecular geometry, electronic properties, and transition states of resveratrol [28, 29], as well as other organic molecules [30–35].

We used vibration analysis to confirm that all optimized geometries correspond to the minimum energy at the same level. The solvent effect analysis on the electronic properties was carried out by the polarizable continuum model (PCM) [36] with the same level of QM calculation.

For sequential Monte Carlo/Quantum Mechanics (s-MC/QM) [37, 38] calculations involving *cis*- and transisomers of resveratrol in both excited and ground states, the rigid structures of the isomers were used. These structures were obtained by reoptimizing each isomer in aqueous solution at the PCM-CAM-B3LYP/6-311+G(d,p) level of QM calculation.

The MC simulations of each isomer in both excited and ground states, surrounded by 1000 water molecules, were performed with the Metropolis sampling technique [39] and standard procedures as presented before [40]. The optimized structure of each isomer was fixed during the MC simulation.



The initial configuration of the isomer solvated by water molecules was generated using a random distribution. The MC simulations were performed in the isothermal-isobaric NPT ensemble, where the number of molecules N, the pressure P, and the temperature T are fixed at N = 1001, P = 1atm, and T = 25 °C. The periodic boundary conditions and the image method were used in a cubic box that was initialized with edge of L = 31.46 Å and the density of  $1 \text{ g/cm}^3$ . During the MC simulation, each molecule interacts with all other within the cutoff radius  $r_c = L/2 = 15.73$  Å. Longrange corrections of Lennard-Jones interactions beyond the cutoff were calculated, as before [40, 41]. The intermolecular interaction was described by the standard Lennard-Jones (LJ) plus Coulomb potentials. For the solutes, the LJ parameters based on the OPLS-AA force field [42] were obtained from LigParGen Web Server [43], and the partial charges were calculated with the CHELPG procedure to fit the electrostatic potential [44] at the CAM-B3LYP/6-311++G(d,p) level of OM calculation, with the solute embedded in aqueous solution described by PCM. For water molecules, interactions were described by simple point charges (SPC) potential developed by van Gunsteren et al. [45]. The MC simulations were performed in two main stages: (i) First, the thermalization stage was executed with  $1.5 \times 10^8$  MC steps until reaching thermodynamic equilibrium; it was followed by (ii) the production stage, comprising  $2.5x10^8$  MC steps, to generate a sufficient number of liquid structures at equilibrium. For the s-MC/QM calculations, we used an average configuration alone (ASEC) obtained from the superposition of 100 MC liquid structures. Hence, a single QM calculation was performed for each isomer using ASEC, which consists of liquid structures obtained from MC simulations with an explicit solute surrounded by its 500 nearest water molecules, represented by normalized point charges. These liquid structures were used to calculate the optical absorption and emission of cis- and trans-isomers of resveratrol in aqueous solution using the s-MC/QM methodology with the CAM-B3LYP/6-311++G level of QM calculation.

NLO effects arise when high-power light interacts with matter. In such a case, the dependence of the electric field on the molecular dipole moment can be expressed in a Taylor series as

$$\mu_{i}(F) = \mu_{i}^{0} + \frac{1}{2} \sum_{j} \alpha_{ij} F_{j} + \frac{1}{2!} \sum_{j,k} \beta_{ijk} F_{j} F_{k} + \frac{1}{3!} \sum_{j,k,l} \gamma_{ijk} F_{j} F_{k} F_{l} \dots$$
(1)

In this equation,  $\mu^0$  is the molecular dipole moment, which is given as

$$\mu^0 = \sqrt{\mu_x^2 + \mu_y^2 + \mu_z^2}. (2)$$

On the other hand,  $\alpha$  is the dipole polarizability, a  $3 \times 3$  tensor that can be combined to give the isotropic and anisotropic contributions

$$\langle \alpha \rangle = \frac{1}{3} (\alpha_{xx} + \alpha_{yy} + \alpha_{zz}), \tag{3}$$

and

$$\Delta \alpha = \sqrt{(\alpha_{xx} - \alpha_{yy})^2 + (\alpha_{xx} - \alpha_{zz})^2 + (\alpha_{yy} - \alpha_{zz})^2}.$$
 (4)

In principle,  $\langle \alpha \rangle$  can be implemented in the Lorentz-Lorenz equation to obtain the refractive index [46, 47]

$$\frac{n^2 - 1}{n^2 + 2} = \frac{4\pi \langle \alpha \rangle}{3V_{mol}},\tag{5}$$

where  $V_{mol}$  is the molecular volume.

The next expansion term is the first hyperpolarizability ( $\beta$ ), i.e., a cubic tensor  $3 \times 3 \times 3$ . In the description of NLO, Hyper-Rayleigh Scattering (HRS), first described by Andrews and Thirunamachandran [48], it is possible to obtain the first frequency-dependent hyperpolarizability,  $\beta(-2\omega;\omega,\omega)$ . The main advantage of this technique is to get the dipole moment ( $\mu$ ) independently and the second hyperpolarizability ( $\gamma$ ), which represents a clear advantage over the second harmonic generation technique induced by an electromagnetic field (EFISGH) if one is interested in obtaining the SHG parameters [49]. Within the HRS formalism

$$\beta_{HRS} = \beta(-2\omega; \omega, \omega) = \sqrt{\langle \beta_{ZZZ}^2 \rangle + \langle \beta_{ZXX}^2 \rangle},$$
 (6)

with

$$\langle \beta_{ZZZ}^{2} \rangle = \frac{1}{7} \sum_{i}^{x,y,z} \beta_{iii}^{2} + \frac{1}{35} \sum_{i \neq j}^{x,y,z} \left( \beta_{iij}^{2} + 4\beta_{jii}^{2} \right)$$

$$+ \frac{2}{35} \sum_{i \neq j}^{x,y,z} \left( \beta_{iii} \beta_{ijj} + 4\beta_{jii} \beta_{iij} + 4\beta_{iii} \beta_{jji} \right)$$

$$+ \frac{1}{105} \sum_{i \neq j \neq k}^{x,y,z} \left( \beta_{iij} \beta_{jkk} + \beta_{iij} \beta_{jkk} + \beta_{ijk} \beta_{jik} \right)$$

$$+ \frac{4}{105} \sum_{i \neq j \neq k}^{x,y,z} \left( \beta_{jii} \beta_{jkk} + 2\beta_{ijk}^{2} \right)$$

$$(7)$$

and

$$\left\langle \beta_{ZXX}^2 \right\rangle = \frac{1}{35} \sum_{i}^{x,y,z} \beta_{iii}^2 + \frac{4}{105} \sum_{i \neq j}^{x,y,z} \left( \beta_{iii} \beta_{ijj} + 2\beta_{iij}^2 \right)$$



$$+\frac{1}{35} \sum_{i \neq j}^{x,y,z} \left( 3\beta_{ijj}^{2} - 2\beta_{iii}\beta_{jji} - 2\beta_{iij}\beta_{jii} \right)$$

$$-\frac{2}{105} \sum_{i \neq j \neq k}^{x,y,z} \left( \beta_{iik}\beta_{jjk} + \beta_{iij}\beta_{jkk} + \beta_{ijk}\beta_{jik} \right)$$

$$+\frac{1}{105} \sum_{i \neq i \neq k}^{x,y,z} \left( 2\beta_{ijk}^{2} + \beta_{ijj}\beta_{jkk} \right)$$
(8)

Within the EFISHG technique, the generation of the second harmonic depends on  $\mu^0$ ,  $\beta_{\parallel}$ , and  $\gamma_{\parallel}$  as

$$\gamma_{EFISHG} = \gamma_{\parallel}(-2\omega; \omega, \omega) + \frac{\mu^{0} \beta_{\parallel}(-2\omega; \omega, \omega)}{3kT}.$$
 (9)

However, as  $\gamma_{\parallel}$  is inexpressible in the face of  $\beta_{\parallel}$ , the SHG effects are often discussed as a function of the product [50, 51].

$$\gamma_{EFISHG} \approx \mu^0 \beta_{\parallel}(-2\omega; \omega, \omega).$$
(10)

In this equation,

$$\beta_{\parallel} = \frac{3}{5} \frac{\vec{\mu^0} \cdot \vec{\beta}_{vec}}{\mu},\tag{11}$$

and

$$\beta_i = \frac{1}{3} \sum_{j}^{x,y,z} (\beta_{ijj} + \beta_{jij} + \beta_{jji}). \tag{12}$$

Concerning the global reactive parameters, the chemical potential  $(\phi)$ , chemical hardness  $(\eta)$ , electrophilicity  $(\omega)$ , and the nucleophilicity (N) are given as

$$\phi = (\varepsilon_L + \varepsilon_H)/2,\tag{13}$$

$$\eta = (\varepsilon_L - \varepsilon_H),\tag{14}$$

and

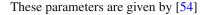
$$\omega = \phi^2 / 2\eta. \tag{15}$$

The nucleophilic index is defined as [52, 53]

$$N = \varepsilon_H - \varepsilon_H^{TCE},\tag{16}$$

where  $\varepsilon_H$  and  $\varepsilon_H^{TCE}$  are the highest molecular orbital (HOMO) energies of the chromophore and tetracyanoethylene (TCE), which is a reference molecule.

The local reactivity parameters are often discussed using the Fukui functions, which describe the selectivity or reactivity of an atomic site or a region in a chemical chromophore.



$$F_k^+ = q_k(N+1) - q_k(N)$$
, for nucleophilic attack (17)

and

$$F_k^- = q_k(N) - q_k(N-1)$$
, for electrophilic attack, (18)

where  $q_k(N)$ ,  $q_k(N+1)$ , and  $q_k(N-1)$  are the electronic populations on the kth atomic site for N, N+1, and N-1 electron systems, respectively. The Fukui functions are combined to give the relative nucleophilic ( $f_{nu} = F_k^+/F_k^-$ ) and electrophilic ( $f_{el} = F_k^-/F_k^+$ ) indexes [54].

If  $f_{nu} > f_{el}$ , the site is inclined to perform a nucleophilic attack on an electrophilic region, but if  $f_{el} > f_{nu}$ , the atomic site will be prone to an electrophilic attack on a nucleophilic site. Finally, all electronic calculations were performed in the Gaussian 09 program [55], but the entire NLO analysis was carried out using the Multiwfn code [56].

#### **Results and discussions**

## **Geometry optimization and properties**

Complete geometry optimization and vibration frequency calculations in gaseous and aqueous environment of the cis (c-Res) and trans (t-Res) conformations of resveratrol were performed using CAM-B3LYP/6-311++G(d, p) QM calculation level. In solution, these calculations were performed using the solvent described by the PCM model with the same level of QM calculation. Gas results for two conformations reveal a nearly planar structure for t-Res, with dihedral angles  $\Phi_1$  (C10-C4-C3-C2) and  $\Phi_2$  (C5-C1-C2-C3) of 9 and 14° (see Fig. 1). The same angles are 37 and 41° for c-Res. With the solvent effect, for example, the water effect, the values of these angles of the c-Res form are almost not altered ( $\Phi_1$  =  $36^{\circ}$  and  $\Phi_2 = 43^{\circ}$ ), but they change significantly for t-Res  $(\Phi_1 = 3^{\circ} \text{ and } \Phi_2 = 4^{\circ})$ , compared to the gas results. This shows that the solvent effect leads to a planar structure for t-Res in water. This result for t-Res agrees well with the Xray data [57] and also provides excellent agreement with the B3LYP and MP2 results obtained using the aug-cc-pVDZ basis set [58].

Table 1 shows the calculated electronic energy, Gibbs free energy, and dipole moment of cis- and trans-optimized structures in gas and water. We identify that both c- and t-Res forms in the gas are stable at the CAM-B3LYP/6-311++G(d,p) level, with the trans form being the most stable in compared to c-Res around 4 kcal/mol. Comparing the free energy in aqueous solution,  $G_{aq}$ , t-Res remains more stable by 5 kcal/mol compared to c-Res. This shows that the solvent improves the relative stability of t-Res compared to gas. It is



**Table 1** The electronic energy ( $E_g$  in kcal/mol), free energy ( $G_g$  in kcal/mol), and the dipole moment ( $\mu_g$  in D) of cis (c-Res) and trans (t-Res) forms in gas were calculated using CAM-B3LYP/6-311++G(d,p)

	$E_g$ (kcal/mol)	$G_g$ (kcal/mol)	$\mu_g (D)$	$E_{aq}$ (kcal/mol)	Gaq (kcal/mol)	$\mu_{aq}(D)$
c-Res	-480796.54	-480679.88	2.54	-480807.00	-480690.32	3.46
t-Res	-480800.20	-480684.02	0.86	-480811.78	-480695.64	0.89
$\Delta$ (cis-trans)	3.66	4.14	1.68	4.78	5.32	2.57

In aqueous solution, the electronic energy  $(E_{aq})$ , the free energies  $(G_{aq})$ , and the dipole moment  $(\mu_{aq})$  were obtained using the solvent described by PCM at the same levels of calculation. Relative values for energies  $(\Delta E \text{ and } \Delta G \text{ in kcal/mol})$  and dipole moments  $(\Delta \mu \text{ in } D)$  are also shown, comparing the cis and trans forms

essential to emphasize that the stability increase of t-Res is not a direct consequence of a change in the dipole moment of the molecule, which varies little (a rise of 0.92 D in c-Res and 0.03 D in t-Res), indicating that the solvent has little effect on the charge redistribution and electronic polarization of the c- and t-Res forms.

By analyzing the atomic charge of c- and t-Res in gas and water, we observe that there are indeed some changes in the calculated charges in water. The most significant difference is in the three oxygen atoms of the hydroxyl groups that have almost the same charge in gas (-0.63 in c-Res and -0.64 int-Res) and in water (-0. 68 in c-Res and -0.70 in t-Res). Thus, the relative stability of t-Res in water is mainly attributed to the structural change in the geometric parameters in the dihedral angles  $\Phi_1$  and  $\Phi_2$  that decrease significantly compared to gas (a 67% decrease in  $\Phi_1$  and 71% in  $\Phi_2$ ) as discussed above. Therefore, we identified that the effect of the solvent on the charge distribution of resveratrol appears to be non-essential but cannot be neglected due to the structural change in geometry caused by the solvent. For this reason, a proper description of the electrostatic interaction of resveratrol requires using the water structure and polarized atomic charges.

# Absorption and emission spectra

The resveratrol absorption spectrum has been of interest for quite some time [60–62], and it increased due to the shape dependence of the spectrum on the conformational changes associated with *cis-trans*, its environment, and its interactions [60, 61]. In an aqueous solution, there are two broad absorption bands in the t-Res spectrum, the first band between 257 and 365 nm and the second band between 200 and 250 nm, with values of  $\lambda_{max}$  around 316 and 216 nm, respectively. In the case of the c-Res spectrum, these two bands change drastically, giving rise to two new bands centered around 290 nm and 227 nm. Thus, in the resveratrol absorption spectra with its *trans-cis* conversion, a blue shift of 26 nm is observed in the first band and a red shift of 11 nm in the second band. The experimental absorption spectra of resveratrol in an aqueous phosphate-borate-SDS buffer solu-

tion reported by Allan et al. [61] and Figueiras et al. [62], and reproduced in this work for comparative purposes, are represented in Fig. 2. The latter showed only the first absorption band of the spectra for both t- and c-Res, which, in the case of t-Res, agrees with that obtained by Allan et al. However, the spectra reported by these works do not agree with the c-Res. In the figure, we also show the absorption spectra of c-Res and t-Res in gas and different solvents (water, DMSO, octanol) obtained using CAM-B3LYP/6-311++G(d, p).

It can be seen from Fig. 2 that for the gas phase, the theoretical absorption spectrum of c-Res is characterized by two bands centered at 279 nm and 213 nm and a shoulder at approximately 253 nm. In the case of the t-Res spectrum,

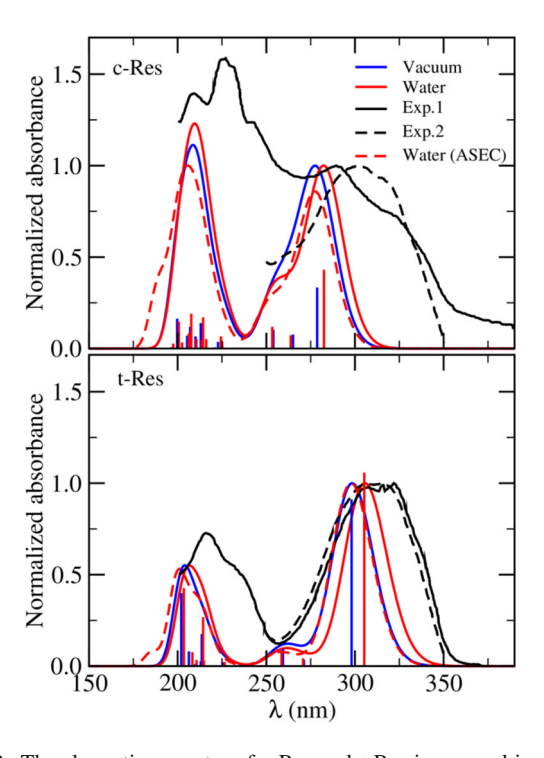


**Fig. 2** The absorption spectra of c-Res and t-Res in gas and in water calculated at the time-dependent formalism using the CAM-B3LYP/6-311++G(d,p) level of QM. We obtained the spectra in water using the Polarizable-Continuum Model (PCM) and ASEC at the same calculation level. Experimental spectra are presented for comparison and were taken from literature [59]



these two bands are identified at 298 and 210 nm, with the shoulder around 260 nm. This result leads to a blue shift of 19 nm in the first band and a red shift of 3 nm in the second band in the *trans-to-cis* isomerization of resveratrol in gas. By comparing the gas and water spectra, it can be seen a redshift for the first absorption band to 282 (278) nm for c-Res and 305 (298) nm for t-Res, increasing the blueshift to 19 nm (gas) at 23 (20) nm (water) with *trans-cis* isomerization, for the solvent described by PCM (ASEC). We observed an excellent agreement of both solvent models: the PCM solvation model, where the solvent is treated as a polarizable continuum medium, and the ASEC model, where the solvent molecules are accounted only as point charges.

These results agree well with the experiments for  $\Delta\lambda$  (trans-cis) of 26 nm [61] and 10 nm [62]. The second band also has a redshift with the gas-to-water change of c- and t-Res. However, this redshift is considerably smaller than the corresponding for the first band, resulting in only 1.0 (1.3) nm increases in  $\Delta\lambda$  (trans-cis) with PCM (ASEC). In the case of non-aqueous solvents (DMSO and octanol), with the solvent described only by PCM, the spectra change very little compared to water, giving almost a superposition between them, with the shoulder being better defined than that of gas. The calculated blueshift,  $\Delta\lambda$  (trans-cis), was approximately 28 and 27 nm, while the redshift was equal to 4 nm. The two lowest absorption maxima and oscillator strength calculated for both c-Res and t-Res in the gas and solvent medium are shown in Table 2.

The calculated spectrum of t-Res generally agrees with experiments [61, 62] and with previous theoretical results [60]. For c-Res, the calculated spectrum deviates from the experimental one in band shape, intensities, and modulus, although the intensities are more difficult to reproduce accurately. Note that the two bands located around 282 (278) nm and 208 (204) nm in the calculated water spectrum with PCM (ASEC) are comparable to those around 290 and 208 nm in the experimental spectrum reported by Allan et al. [61].

Furthermore, to better understand the optical properties of resveratrol and, in particular, its first band blue shift with trans-cis isomerization, we calculated the emission spectra in gas and solvent medium. Considering the relaxation of the first excited state, we calculated the emission spectra of c- and t-Res for their fully and partially optimized structures. These partially optimized structures are not completely relaxed and are obtained from the geometry optimization process, where intermediate systems with the spectra that best agree with the experimental ones are chosen. Figure 3 compares the absorption and emission spectra (for partially and fully optimized structures) of c- and t-Res in an aqueous solution. The main emission band in the calculated t-Res spectra for partially optimized structures is around 396 (375) nm, whereas for the c-Res spectrum, this band is around 386 (424) nm obtained with PCM (ASEC). It can be seen from Fig. 3 that the emission band for fully optimized structures shows discrepancies of 29 (1) nm for t-Res and 214 (104) nm for c-Res, compared to partially structures.

**Table 2** The wavelength (nm) and oscillator force (f) calculated for the absorption and emission spectra of two primary intense excitations of c-and t-Res in gas and different solvents

		Gas	Gas		Octanol			Water		Exp. [61, 62]
	Trans	λ	f	λ	f	λ	f	λ	f	λ
Absorption spectra (AS), $\lambda_{ab}$										
c-Res	1 <sup>st</sup>	278.7	0.3	282.8	0.5	282.4	0.5	282.5 (277.7)	0.4 (0.4)	302 (290)
	2 <sup>nd</sup>	213.0	0.1	208.6	0.2	208.1	0.2	207.7 (204.1)	0.2 (0.2)	227
t-Res	1 <sup>st</sup>	298.1	0.9	309.6	1.1	309.9	1.1	305.2 (297.5)	1.1 (0.9)	311 (316)
	2 <sup>nd</sup>	209.8	0.0	204.3	0.4	204.1	0.4	203.5 (199.7)	0.4 (0.4)	216
Δλ (cis-trans)										
Blue shift	1 <sup>st</sup>	19.4		26.8		27.5		22.7 (19.8)		9 (26)
Red shift	2 <sup>nd</sup>	-3.2		-4.4		-3.9		-4.2 (-4.5)		-11
Emission spectra (ES), $\lambda_{em}$										
c-Res	1 <sup>st</sup>	379.6	0.1	382.8	0.4	384.3	0.4	385.5 (423.9)	0.4 (0.5)	372
t-Res	1 <sup>st</sup>	350.4	0.9	392.0	1.2	398.4	1.3	396.1 (374.8)	1.3 (1.0)	393
Δλ (cis-trans)										
Blue shift	1 <sup>st</sup>	-29.2		9.2		14.1		10.6 (-49.1)		21
$\Delta\lambda$ (ES-AS) - Stokes shift										
c-Res	1 <sup>st</sup>	100.9		100.0		101.9		103.0 (146.3)		70
t-Res	1 <sup>st</sup>	52.3		82.4		88.5		90.9 (77.3)		82

Results were obtained using PCM-CAM-B3LYP/6-311++G(d, p) and in parentheses using ASEC with the same level of QM calculation



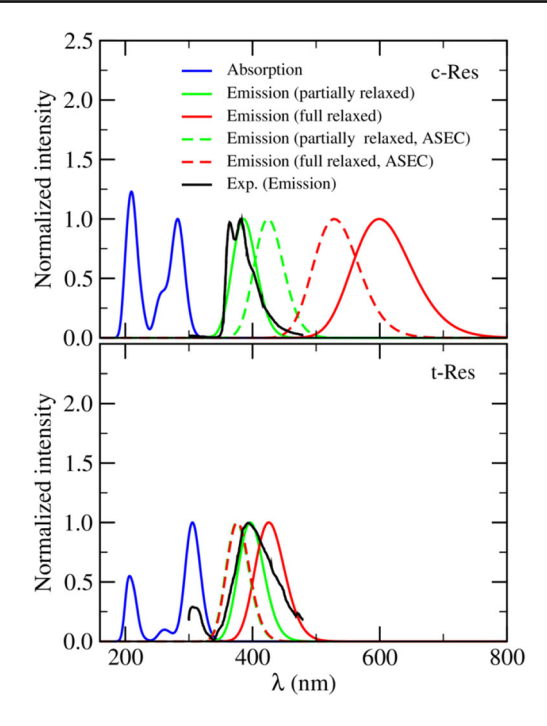


Fig. 3 Emission spectra of c-Res and t-Res in water obtained using CAM-B3LYP/6-311++G(d,p) level of QM, with the solvent described by PCM and ASEC. For comparison, the experimental spectra [62] reproduced in this work are also shown

It is also worth noting that *trans-cis* isomerization causes a different behavior in the emission spectrum of the analyzed structures. We observed a blue shift of 10 nm partially and a red shift of 175 nm for all optimized structures using the PCM model. The solvation model ASEC gives a red shift of 49 nm for partially and 152 nm for fully optimized structures. Both solvation models, PCM and ASEC, showed reasonable agreement with the experimental results for absorption spectra. However, the ASEC exhibited inaccuracies in the emission study, predicting a red shift for isomerization in both partially and fully optimized structures (see Table 2). Therefore, we observe that the values obtained with the partially optimized systems using the PCM model give the best estimation for both  $\lambda_{em}$  and  $\Delta\lambda$  (cis-trans). This blue shift observed in both absorption and emission resveratrol spectra plays a vital role in studying the kinetics of trans-cis isomerization, which can be used to monitor the increase in c-Res concentration upon continuous excitation of t-Res samples. These calculated blue shifts of 22.7 and 10.0 nm in the absorption and emission spectra with PCM model are a direct consequence of the energy gap between the ground state and the excited state, which is broader for c-Res (85.3 kcal /mol) than for t-Res (78.9 kcal/mol). It is essential to note that this result was obtained using partially optimized structures with PCM model. For complete optimized systems, the energy gap was wider for t-Res than for c-Res, predicting a red shift in the absorption and emission spectra in disagreement with the experiment (see Fig. 4). Therefore, we adopt the values obtained with partially optimized structures as our best results for emission. Hence, using the calculations obtained for the absorption spectra, we can predict a significant Stokes shift of 91 and 103 nm for the tand c-Res structures, which give reasonable agreement with the experimental values of 82 and 70 nm, respectively. The behavior for the changes in the resveratrol spectrum in its *trans-cis* conversion is supported for the spectrum calculated in non-aqueous solvents (DMSO and octanol), where we obtained values for the blue shift and the Stokes shift with the same order of magnitude of those obtained for water, see Table 2.

# Dipole polarizability and refractive index analysis

Table 3 presents the NLO results obtained at the CAM-B3LYP/6-311++G(d,p) level of quantum mechanics for the cis and trans isomers in gas and different solvent environments. In the gas phase, the isotropic polarizability of trans isomer,  $29.19 \times 10^{-24}$  esu, has an improved response than its counterpart ,  $26.56 \times 10^{-24}$  esu (see Fig. 5). The same behavior is observed for the anisotropic term ( $\Delta \alpha$ ), which presents  $22.10 \times 10^{-24}$  and  $22.10 \times 10^{-24}$  esu, respectively, for trans and conformers. Such a behavior is a consequence

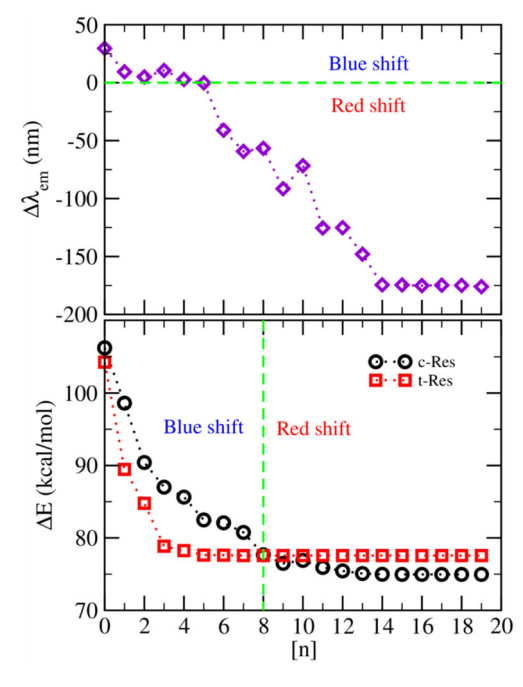
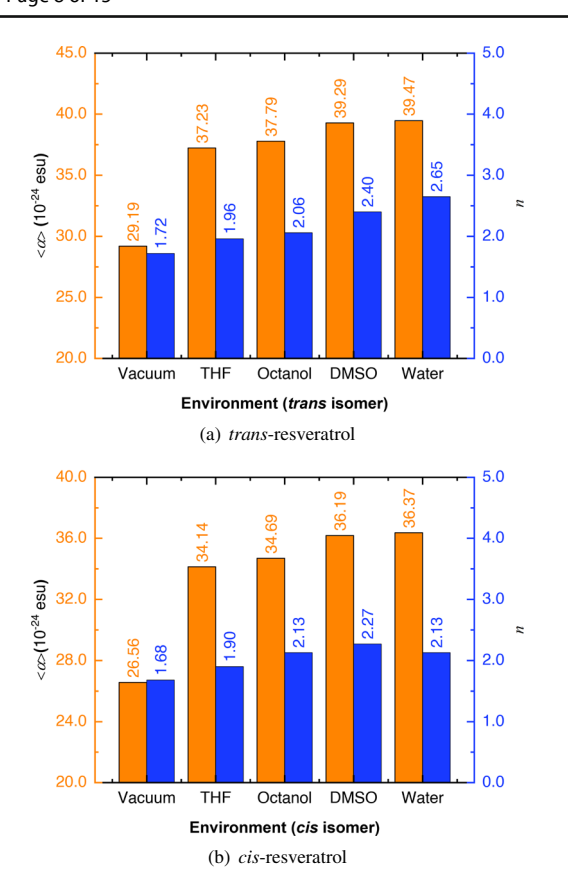


Fig. 4 The wavelength difference between the cis and trans isomers ( $\Delta cis$ -trans) in the emission spectra of resveratrol in water (top) and its energy gap between the ground state and excited state ( $\Delta E$ ) (bottom) calculated during geometry optimization of the cis and trans isomers in the excited state in the same solvent using CAM-B3LYP/6-311++G(d,p) level of QM, with the solvent described by PCM





**Fig. 5** The behavior of the  $\langle \alpha \rangle$ ,  $\Delta \alpha$ , and *n* concerning the increase of the solvent polarity

of induced changes in the molecular eigenstates due to the polarization of the solute due to the solvent.

**Table 3** Isotropic ( $\langle \alpha \rangle/10^{-24}$  esu) and anisotropic ( $\Delta \alpha/10^{-24}$  esu) contributions for the static dipolar polarizability, and the dynamic ( $\lambda = 1907$  nm) HRS and EFISHG responses ( $\beta_{HRS}/10^{-30}$  esu, and  $\beta_{\parallel}/10^{-30}$  esu, and  $\mu \beta_{\parallel}/10^{-48}$  esu), and HOMO ( $\varepsilon_H/\text{eV}$ ) and LUMO

In addition, the *trans* isomer presents other remarkable characteristics, i.e., the isotropic contribution is smaller than the anisotropic one,  $\langle \alpha \rangle - \Delta \alpha < 0$ , and the opposite statement is true for its counterpart,  $\langle \alpha \rangle - \Delta \alpha > 0$ . For example, this behavior has been reported in azo dyes [7].

Along the Lorentz-Lorenz equation, one can connect the polarizability of the dipole with the refractive [46, 47], which gives the ratio between the speed of light in a gas and the insolvent (n=c/v). Thus, if efficient data transport is desired, the idea is to obtain systems with lower refractive indices. After analyzing Table 3, it is observed that strong polar solvents increase the value of n. For example, this statement can be confirmed by comparing the values of n for the structures in gas (n=1.68) and in solvent water (n=2.13), which corresponds to an increase of ca. 26% (see Fig. 5). However, less polar solvents such as THF (n=1.90) present values closer to those obtained in a gas. Furthermore, the structure has lower refractive indices than the *trans* isomers. This fact means that the best optical transport system should consider -resveratrol solvated in low polarity solvents.

# First hyperpolarizability and the second-harmonic generation

Table 3 also presents the results obtained for the first frequency-dependent hyperpolarizabilities ( $\beta_{HRS}$ ) obtained using the Hyper-Rayleigh scattering technique [63]. This tensor is the most relevant NLO parameter and is responsible for the second harmonic generation phenomenon [63]. At first, it can be observed that the hyperpolarizability obtained from the *trans* conformation is greater than the value obtained for

 $(\varepsilon_L/eV)$  energies, chemical potential  $(\phi/eV)$ , chemical hardness  $(\eta/eV)$ , electrophilicity  $(\omega/eV)$ , and nucleophilicity (N/eV) of resveratrol in different mediums obtained using CAM-B3LYP/6-311++G(d,p) level of QM calculation

	Gas ( $\varepsilon = 1.00$ )		THF ( $\varepsilon = 7.42$ )		Octanol ( $\varepsilon = 9.86$ )		DMSO ( $\varepsilon = 46.83$ )		Water ( $\varepsilon = 78.35$ )	
Property	cis	trans	cis	trans	cis	trans	cis	trans	cis	trans
$\langle \alpha \rangle$	26.56	29.19	34.14	37.23	34.69	37.79	36.19	39.29	36.37	39.47
$\Delta \alpha$	22.10	41.67	25.56	51.69	25.51	52.07	25.15	52.93	25.08	53.01
n	1.68	1.72	1.90	1.96	2.13	2.06	2.27	2.40	2.13	2.65
$\beta_{HRS}$	3.36	10.00	5.12	16.31	5.21	16.66	5.21	16.85	4.94	15.00
$oldsymbol{eta}_{\parallel}$	1.29	10.28	2.62	19.50	2.69	20.13	2.73	21.25	2.59	20.31
$\mu eta_\parallel$	3.17	8.84	8.48	18.75	8.86	19.30	9.09	19.80	8.67	18.05
$\varepsilon_H$	-7.22	-6.97	-7.26	-7.03	-7.27	-7.03	-7.29	-7.05	-7.29 (-7.45)	-7.08 (-7.38)
$arepsilon_L$	-0.21	-0.47	-0.25	-0.57	-0.25	-0.58	-0.26	-0.60	-0.28 (-0.41)	-0.58  (-0.88)
$\phi$	-3.71	-3.72	-3.75	-3.80	-3.76	-3.80	-3.78	-3.82	-3.79(-3.93)	-3.83 (-4.13)
$\eta$	7.01	6.50	7.01	6.46	7.02	6.45	7.03	6.45	7.01 (7.04)	6.50 (6.50)
ω	0.98	1.06	1.01	1.12	1.01	1.12	1.01	1.13	1.02 (1.10)	1.13 (1.31)
N	3.77	4.02	3.39	3.62	3.36	3.60	3.29	3.53	3.29 (3.13)	3.50 (3.20)

In solution, the values were calculated using the PCM solvation model and in parenthesis using ASEC at the same level of QM calculation



the isomer. This effect has been reported for other dyes [7] and has connections with the topology of the frontier molecular orbitals and the energy gap between them. In Fig. 6, it can be seen that the *trans* isomer overlaps better with the HOMO and LUMO, which favors charge transfer, polarizations, and decreases the HOMO-LUMO energy gap. As shown above, there is an inverse relationship between the first hyperpolarizability and the energy gap ( $\Delta\beta \propto \Delta E_g^{-n}$ ) [64, 65]. This is the resveratrol structure change effect from to *trans*. For example, under gas phase conditions, the energy gap from to *trans* decreases by 0.51 eV, while  $\beta_{HRS}$  increases by 6.64 × 10<sup>-30</sup> esu, ca. 198%.

On the other hand, the solvent effect on  $\beta_{HRS}$  is the most interesting problem. According to the two-level model proposed by Oudar and Chemla [66] and later confirmed by Zyss [67], the first hyperpolarizability presents a strong dependence on the dipole moment of the excited state.

$$\beta_{tl} \propto \frac{\Delta \mu f}{\Delta E_g^3}.\tag{19}$$

In such an equation, f is the oscillator strength of electronic excitation,  $\Delta E_g$  is the energy gap mentioned above, and  $\Delta \mu = \mu_e - \mu_g$  is the difference between the excited state dipole moment and its corresponding ground state.

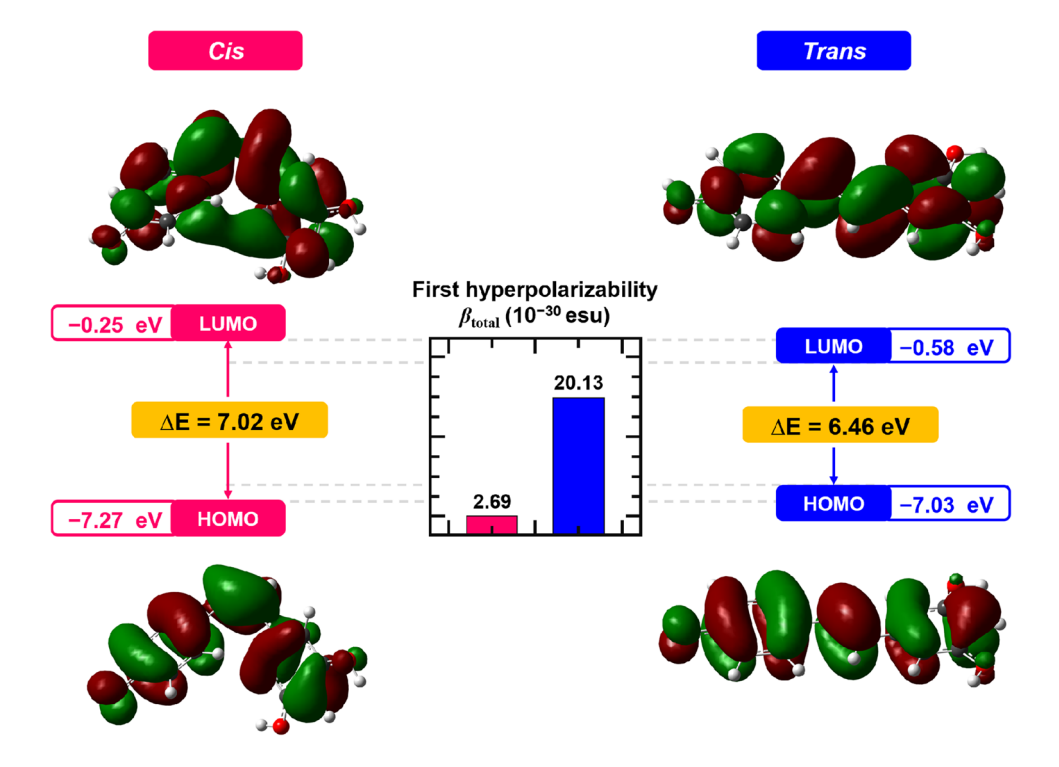
Thus, resveratrol presents a well-defined hypsochromism when the polarity of the medium increases. According to Reichardt [1], this effect is caused by the difference between the dipole moments of the terrestrial and excited state. When  $\mu_e$  is less than  $\mu_g$ , a blue shift (hypsochromism) is observed

in the electronic emission and absorption spectra. This effect occurs for *cis*-isomer of resveratrol [19], and our current calculations on the excited and ground states indicate that the dipoles are respectively 6.19 and 2.54 D. As a consequence, Eq. 19 predicts a decrease in the first hyperpolarization when the polarity of the solvent increases, and this effect occurs. For example, from octanol to water, the dielectric constant increases from  $\varepsilon=9.86$  to  $\varepsilon=78.35$ , but the first hyperpolarizability obtained for the *trans* isomer decreases from  $16.66\times10^{-30}$  to  $10.00\times10^{-30}$  esu, which represents a 40% reduction in the optical response. A similar behavior is found for the *cis* structure. The solvent has a considerable impact on the NLO response of resveratrol.

Comparison with other molecular systems is inevitable. Recently, a family of thieno[3,4-*b*]pyrazine derivatives have been synthesized [68], and their NLO properties have been carefully analyzed [50]. These  $\pi$  conjugate systems exhibited frequency-dependent hyperpolarizabilities ranging from  $0.49 \times 10^{-30}$  to  $52.56 \times 10^{-30}$  esu. Compared to urea, which is another NLO chromophore, static hyperpolarizabilities ( $\beta_{total}$ ) of  $0.34 \times 10^{-30}$  esu [69] have been reported. These results indicate that resveratrol could be promising for optical applications.

However, estimating the first hyperpolarization is incomplete in determining a material NLO behavior. However, frequency-dependent hyperpolarization can be used to estimate the main contributions to the third-order EFISHG response [50, 51]. The theoretical parameters ( $\beta_{\parallel}$  and  $\mu^0\beta_{\parallel}$ ) necessary to estimate the behavior of the GAA are shown in Table 3. For the solvated cis isomer,  $\beta_{\parallel}$  varies from

**Fig. 6** The frontier molecular orbitals, energy gap ( $\Delta E_g$ ), and frequency-dependent first hyperpolarizability ( $\beta_{HRS}$ ) calculated at CAM-B3LYP/6-311++G(d,p) for the and trans structures in an aqueous environment using the solvent modeled with PCM





 $2.59 \times 10^{-30}$  to  $2.73 \times 10^{-30}$  esu, depending on the choice of solvent (see Fig. 7). These values are only three times smaller than those estimated for other NLO materials such as the *p*-nitroaniline molecule, (*p*-NA) with  $\beta_{\parallel} = 6.73 \times 10^{-30}$  esu [70].

The IEFSGH gives results related to the product  $\mu^0\beta_\parallel$ . Consequently, there is a dependence on the dipole moment of the ground state. As can be seen, the *cis* structure presents a lower IEFSHG response than its corresponding *trans*. For example, under gas phase conditions,  $3.17 \times 10^{-48}$  and  $8.84 \times 10^{-48}$  are obtained for the *cis* and *trans* conformations, and this behavior does not depend on the environment. However, for less polar solvents, the product increases significantly. For example, in the solvent octanol, the conformer under *trans*-isomerization exhibits a second harmonic behavior of  $19.30 \times 10^{-48}$  esu, i.e., an increase of ca. 118%. These values are smaller, but again, they compete well with those reported for p-NA ( $\mu^0\beta_\parallel = 48.5 \times 10^{-48}$  esu) [70].

# **Global reactivity descriptors**

Global and local reactivity descriptors are a set of parameters that provide information about the reactivity and toxicity of a drug candidate. The former parameters,  $\phi$ ,  $\eta$ ,  $\omega$ , and N, present in Table 3, depend only on the energies of the

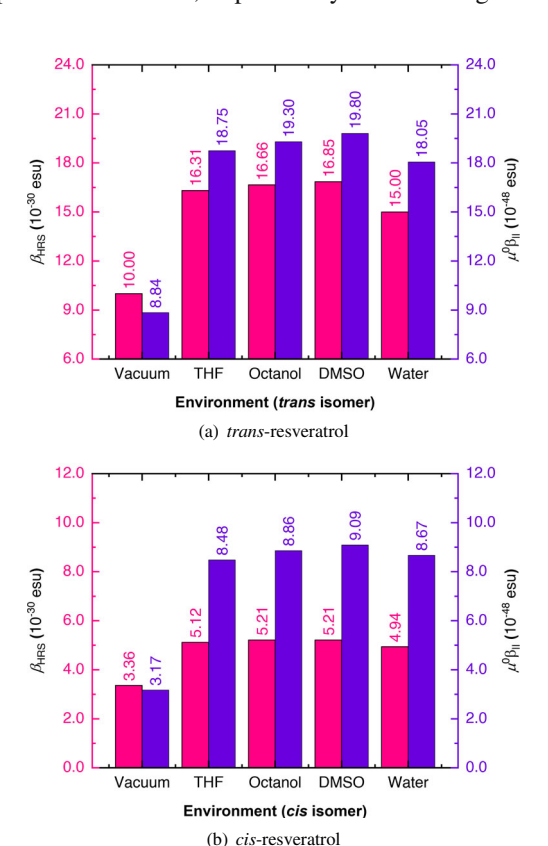


Fig. 7 The behavior of the  $\beta_{HRS}$  and  $\mu^0\beta_\parallel$  concerning the increase of the solvent polarity



frontier molecular orbitals of the chromophore. The chemical potential,  $(\phi)$ , shows negligible dependence in the gas phase on *cis-trans* isomerization according to DFT calculations performed in gas, for example,  $\phi^{cis} = -3.71$  eV while  $\phi^{trans} = -3.72$  eV. Meanwhile, the solvent acts in two ways: First, the environment makes both isomers, *cis* and *trans*, more stable than in the gas phase. Second, every investigated solvent makes the *trans* isomer more stable than its *cis* counterpart,  $\phi^{trans} > \phi^{cis}$ .

Chemical hardness ( $\eta$ ) describes the degree of polarization that a chromophore can undergo. Large values of hardness indicate low isotropic polarizability of the material electronic structure, obeying a linear decay relationship such as  $\eta = A\langle \alpha \rangle + B$  [50, 71, 72].

Regarding isomerization,  $\eta^{cis} > \eta^{trans}$  independent of the environment, which indicates that the cis structure is less polarizable than the trans one, such a statement agrees with the results obtained for dipole polarizability in which  $\langle \alpha \rangle^{cis} < \langle \alpha \rangle^{trans}$ . Regarding the solvent effect, analyzing the solvent contribution to the cis conformation, it increases the chemical hardness, obtaining a positive variation ( $\Delta \eta^{cis} > 0$ ) from gas to octanol, following the result that the polarizability of the dipole must, for example, decrease. The trans structure, on the other hand, has the opposite behavior, i.e.  $\Delta \eta^{trans} < 0$ .

For a pharmacy candidate, it is vital to determine the degree of chromophore electrophilicity since when a xenobiotic electrophile interacts with proteins, it is possible to cause cellular toxicity or an immune reaction, as occurs with vaccines [58]. However, if these interactions occur with nucleic acids, a genetic mutation or a carcinogenic process can be observed, which should be avoided [73]. Concerning overall electrophilicity, Domingo and his collaborators proposed a scale that organizes a chromophore as weak ( $\omega < 0.8 \text{ eV}$ ), moderate (0.8  $\leq \omega \leq$  1.5 eV), or intense ( $\omega >$  1.5 eV) electrophile [74]. When analyzing the results for resveratrol, it is observed that both the cis and trans structures are classified as moderate electrophiles. However, the trans isomer has higher ratios for the cis conformer. For example, in the gas phase, DFT results indicate values of 0.98 and 1.06 eV for resveratrol cis and trans, respectively. Regarding the solvent effect, the results indicate that the environment gently increases the electrophilic characteristic of the chromophore. For example, from gas to octanol,  $\omega$  increases less than 6%.

Regarding global nucleophilicity (N), there is an empirical scale that allows classifying a chromophore as weak (N < 2.0 eV), moderate  $2.0 \le N \le 3.0 \text{ eV})$ , and strong (N > 3.0 eV) nucleophile. Immediately from Table 3, it is seen that resveratrol is a strong nucleophile. For example, the isomers cis and trans have values of  $N^{cis} = 3.77$  and  $N^{trans} = 4.02 \text{ eV}$ , respectively. However, unlike electrophilicity, the solvent acts by decreasing the overall nucleophilicity. As another example, one can examine the transition from gas

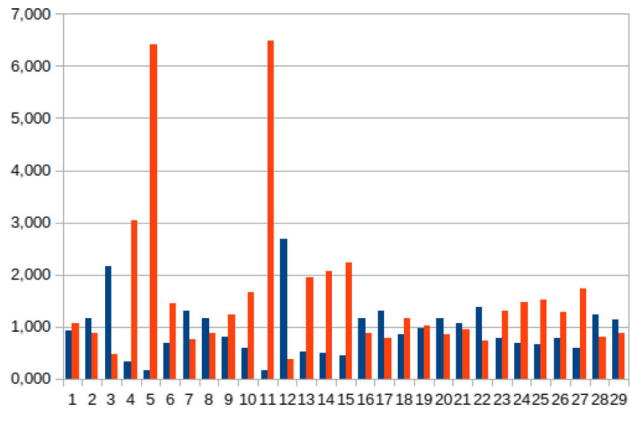
 $(N^{cis} = 3.77 \text{ eV})$  to solvent water  $(N^{cis} = 3.29 \text{ eV})$  for the cis structure, which means a solvent effect of 13%.

### **Fukui functions**

In a biological environment, a pharmacological candidate interacts with an enzyme or a protein through specific interactions such as hydrogen bonds or van der Waals forces. This interaction depends on the electrophilic/nucleophilic character of the chromophore atomic site. The role played by an individual atomic site is easily determined by analyzing the nucleophilic ( $f_{nu}$ ) and electrophilic ( $f_{el}$ ) indices (see Fig. 8 and Table 4) obtained by manipulating the Fukui functions.

**Table 4** The electrophilic ( $f_{el}=F^-/F^+$ ) and nucleophilic ( $f_{nu}=F^+/F^-$ ) dimension less indexes obtained from the Fukui functions at the CAM-B3LYP/6-311++G(d,p) level of quantum mechanics with PCM simulating octanol solvent

	trans		cis	
Atom	$f_{nu}$	$f_{el}$	$f_{nu}$	$f_{el}$
C1	0.931	1.075	2.218	0.451
C2	1.156	0.865	1.522	0.657
C3	2.150	0.465	0.626	1.597
C4	0.328	3.049	0.081	12.382
C5	0.156	6.420	66.098	0.015
C6	0.688	1.454	1.672	0.598
C7	1.311	0.763	1.747	0.572
C8	1.152	0.868	0.355	2.818
C9	0.815	1.227	1.540	0.649
C10	0.599	1.671	0.716	1.397
C11	0.154	6.481	0.297	3.365
C12	2.672	0.374	4.074	0.245
C13	0.512	1.955	0.401	2.492
C14	0.483	2.068	1.322	0.757
O15	0.450	2.220	0.354	2.828
O16	1.153	0.867	1.362	0.734
O17	1.297	0.771	1.274	0.785
H18	0.864	1.158	1.529	0.654
H19	0.980	1.021	1.349	0.741
H20	1.159	0.863	1.653	0.605
H21	1.057	0.946	1.348	0.742
H22	1.364	0.733	1.846	0.542
H23	0.771	1.297	0.494	2.023
H24	0.686	1.458	0.582	1.717
H25	0.661	1.512	0.556	1.799
H26	0.785	1.273	0.856	1.169
H27	0.580	1.723	0.471	2.124
H28	1.232	0.812	2.197	0.455
H29	1.139	0.878	1.521	0.657



(a) trans-resveratrol

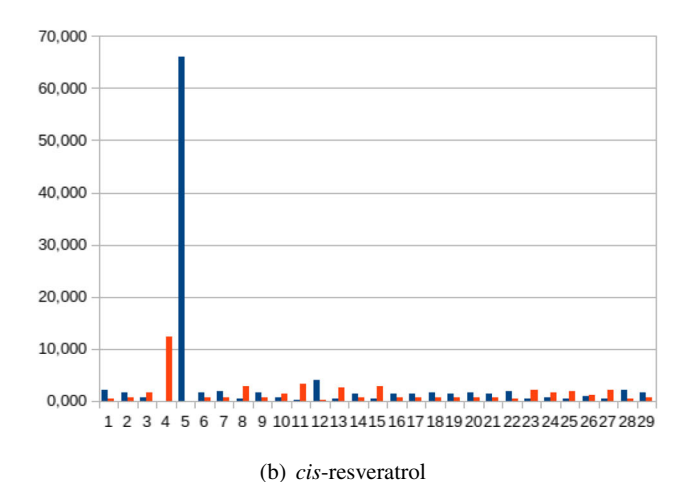


**Fig. 8** The electrophilic ( $f_{el}$  in red color) and nucleophilic ( $f_{nu}$  in blue color) indexes obtained using the CAM-B3LYP/6-311++G(d,p) level of quantum mechanics in octanol solvent

The results suggest that isomerization does not significantly affect the reactive character of oxygen atoms when the system migrates from *trans* to *cis* structures. For example, Fig. 8 shows that O15 has an electrophilic behavior  $(f_{el} > f_{nu})$  in both the *cis* and *chromophores trans*. However, the O16 and O17 sites are prone to nucleophilic attack  $(f_{nu} > f_{el})$ .

Different behaviors are observed for carbon and hydrogen atoms. In the former, the carbons are in the azo bridge, and C2 and C3 exhibit nucleophilic behavior, which is expected considering the high electron density characteristic of the  $\pi$  bridge featured for azo moiety, nevertheless, when the system transitions to cis conformation, the twist puts C3 at an electrophilic site, indicating that isomerization affects the electron density and changes the reactive characteristic of the azo backbone.

Even so, in the carbon atoms, some elements placed in the aromatic rings (C5, C6, C9, and C14) have an electrophilic



character that changes to a nucleophilic site when resveratrol changes from *trans* to *conformation*. *cis*. On the other hand, C8 is a nucleophilic atom but changes its characteristic to electrophilic in the *cis* conformed.

Isomerization also affects the hydrogen atoms located in the azo bridge. *trans* structures H19 and H20 are electrophilic sites. However, the system changes to *cis* structure, making them nucleophiles, while the other hydrogens, H20-H29, maintain their electrophilic or nucleophilic characteristics, as shown in Fig. 8.

# **Conclusions**

A detailed discussion on the contributions of solvents to the stability, reactivity, and NLO response of resveratrol was carried out using the DFT method and continuous solvation models. Between the main findings, we can mention that although the *trans* structure is the most stable chromophore, it is demonstrated that the *cis-trans* barrier can be photoinduced by the light of higher frequencies, allowing the *cis-trans*activation in a variety of solvents.

Concerning solvatochromism, unlike other dyes, resveratrol shows an unusual blue shift (hypsochromic effect) in environments of increasing polarity. According to TD-DFT calculations using both continuous and explicit solvation models, this effect depends on the charge transfer processes and the dipole moment of the excited state. Finally, the studied chromophore presents considerable potential for generating the second harmonic, with a performance comparable to that of some NLO materials such as urea, *p*-nitroaniline, and some selected chalcones. However, unlike these materials, the best response occurs with low polarity solvents such as octanol, which improves ca. 67% the response of NLO concerning the gas phase condition.

Author Contributions Igo T. Lima: electronic structure calculations, data analysis, writing. Ramon F. C. Gomes: electronic structure calculations, data analysis. Edson N. C. Paura: electronic structure calculations, data analysis. Rodrigo Gester: formal analysis, writing—original draft. Patricio F. Provasi: formal analysis, writing—original draft. Antonio R. da Cunha: writing—original draft, writing—review and editing, supervision.

Funding FAPEMA (Fundação de Amparo à Pesquisa e ao Desenvolvimento Científico e Tecnológico do Maranhão) has supported Ramon F. C. Gomes, Edson N. C. Paura, and Antonio R. da Cunha — FAPESP (Fundação de Amparo a Pesquisa do Estado São Paulo) has supported Antonio R. da Cunha — CNPq (Conselho Nacional de Desenvolvimento Científico e Tecnológico) has supported Igo T. Lima, Ramon F. C. Gomes Edson N. C. Paura, Rodrigo Gester and Antonio R. da Cunha.

Availability of data and material Not applicable.

Code availability Not applicable.



### **Declarations**

Conflict of interest All authors declare that they have no competing interests.

### References

- Reichardt C, Welton T (2010) Solvent effects on the absorption spectra of organic compounds, John Wiley & Sons Ltd. Ch. 6:359– 424. https://doi.org/10.1002/9783527632220.ch6
- Abdillah A, Sonawane PM, Kim D, Mametov D, Shimodaira S, Park Y, Churchill DG (2021) Discussions of fluorescence in selenium chemistry: recently reported probes, particles, and a clearer biological knowledge. Molecules 26(3):692. https://doi.org/10. 3390/molecules26030692
- Paisley NR, Halldorson SV, Tran MV, Gupta R, Kamal S, Algar WR, Hudson ZM (2021) Near-infrared-emitting borondifluoride-curcuminoid-based polymers exhibiting thermally activated delayed fluorescence as biological imaging probes. Angewandte Chemie 60(34):18630–18638. https://doi.org/10.1002/ anie.202103965
- Cao H, Pan X, Li C, Zhou C, Deng F, Li T (2003) Density functional theory calculations for resveratrol. Bioorg Med Chem Lett 13(11):1869–1871. https://doi.org/10.1016/S0960-894X(03)00283-X
- Mikulski D, Szelag M, Molski M, Górniak R (2010) Quantumchemical study on the antioxidation mechanisms of transresveratrol reactions with free radicals in the gas phase, water and ethanol environment. J Mol Struct THEOCHEM 951(1):37–48. https://doi.org/10.1016/j.theochem.2010.04.005
- Manzoni V, Modesto-Costa L, Nero JD, Andrade-Filho T, Gester R (2019) Strong enhancement of NLO response of methyl orange dyes through solvent effects: a sequential Monte Carlo/DFT investigation. Opt Mater 94:152–159. https://doi.org/10.1016/j.optmat. 2019.05.018
- Raiol A, da Cunha AR, Manzoni V, Andrade-Filho T, Gester R (2021) Solvent enhancement and isomeric effects on the NLO properties of a photoinduced cis-trans azomethine chromophore: a sequential MC/QM study. J Mol Liq 340:116887. https://doi.org/ 10.1016/j.molliq.2021.116887
- Ro JH, Liu CC, Lin MC (2020) Resveratrol mitigates cerebral ischemic injury by altering levels of trace elements, toxic metal, lipid peroxidation, and antioxidant activity. Biol Trace Elem Res 199(10):3718–3727. https://doi.org/10.1007/s12011-020-02497-
- Annaji M, Poudel I, Boddu SHS, Arnold RD, Tiwari AK, Babu RJ (2021) Resveratrol-loaded nanomedicines for cancer applications. Cancer Rep 4(3). https://doi.org/10.1002/cnr2.1353
- Marinheiro D, Ferreira B, Oskoei P, Oliveira H, Silva AD (2021) Encapsulation and enhanced release of resveratrol from mesoporous silica nanoparticles for melanoma therapy. Materials 14(6):1382. https://doi.org/10.3390/ma14061382
- Risuleo G, La Mesa C (2021) Chapter 33 biological activities and potential nanotechnological delivery of resveratrol, in: Nutraceuticals (Second Edition), second edition Edition, Academic Press, pp 519–536. https://doi.org/10.1016/B978-0-12-821038-3.00033-1
- Cai YJ, Fang JG, Ma LP, Yang L, Liu ZL (2003) Inhibition of free radical-induced peroxidation of rat liver microsomes by resveratrol and its analogues. Biochim Biophys Acta (BBA) - Mol Basis Dis 1637(1):31–38. https://doi.org/10.1016/S0925-4439(02)00174-6

- 13. Surh YJ, Hurh YJ, Kang JY, Lee E, Kong G, Lee SJ (1999) Resveratrol, an antioxidant present in red wine, induces apoptosis in human promyelocytic leukemia (HL-60) cells. Cancer Lett 140(1):1–10. https://doi.org/10.1016/S0304-3835(99)00039-7
- Pace-Asciak CR, Hahn S, Diamandis EP, Soleas G, Goldberg DM (1995) The red wine phenolics trans-resveratrol and quercetin block human platelet aggregation and eicosanoid synthesis: implications for protection against coronary heart disease. Clin Chim Acta 235(2):207–219. https://doi.org/10.1016/0009-8981(95)06045-1
- Lorenz P, Roychowdhury S, Engelmann M, Wolf G, Horn TFW (2003) Oxyresveratrol and resveratrol are potent antioxidants and free radical scavengers: effect on nitrosative and oxidative stress derived from microglial cells. Nitric Oxide 9(2):64–76. https://doi.org/10.1016/j.niox.2003.09.005
- Jang M, Cai L, Udeani GO, Slowing KV, Thomas CF, Beecher CWW, Fong HHS, Farnsworth NR, Kinghorn AD, Mehta RG, Moon RC, Pezzuto JM (1997) Cancer chemopreventive activity of resveratrol, a natural product derived from grapes. Science 275(5297):218–220. https://doi.org/10.1126/science.275.5297.218
- Thuy PT, The SN (2020) Antioxidant of trans-resveratrol: a comparison between OH and CH groups based on thermodynamic views. J Chem 2020:8869023. https://doi.org/10.1155/ 2020/8869023
- Bhat KP, Kosmeder JW, Pezzuto JM (2001) Biological effects of resveratrol. Antioxidants & Redox Signaling 3(6):1041–1064. https://doi.org/10.1089/152308601317203567
- Mazzone G, Malaj N, Russo N, Toscano M (2013) Density functional study of the antioxidant activity of some recently synthesized resveratrol analogues. Food Chem 141(3):2017–2024. https://doi.org/10.1016/j.foodchem.2013.05.071
- Manfredi C, Trifuoggi M, Amoresano A, Vasca E, Pepe C, Volino S, Annetta M (2017) On trans-resveratrol in aqueous solutions.
   J Sol Chem 46(12):2214–2230. https://doi.org/10.1007/s10953-017-0693-9
- Leulescu M, Rotaru A, Moanţă A, Iacobescu G, Pălărie I, Cioateră N, Popescu M, Criveanu MC, Morîntale E, Bojan M, Rotaru P (2021) Azorubine: physical, thermal and bioactive properties of the widely employed food, pharmaceutical and cosmetic red azo dye material. J Thermal Anal Calorimetry 143(6):3945–3967. https:// doi.org/10.1007/s10973-021-10618-4
- Qi S, Zhang C, Yang X, Chen K, Zhang L, Wang X, Xu T, Tian J, Zhang G (2004) Experimental study of photoinduced birefringence in azo-dye-doped polymer. Optik 115(6):253–256. https://doi.org/ 10.1078/0030-4026-00354
- Hohenberg P, Kohn W (1964) Inhomogeneous electron gas. Phys Rev 136(3B):B864–B871. https://doi.org/10.1103/physrev. 136.b864
- Kohn W, Sham LJ (1965) Self-consistent equations including exchange and correlation effects. Phys Rev 140(4A):A1133– A1138. https://doi.org/10.1103/physrev.140.a1133
- Parr RG, Weitao Y (1994) Density-functional theory of atoms and molecules. Oxford University Press, USA
- Yanai T, Tew DP, Handy NC (2004) A new hybrid exchangecorrelation functional using the coulomb-attenuating method (CAM-B3LYP). Chem Phys Lett 393(1):51–57. https://doi.org/10. 1016/j.cplett.2004.06.011
- Ditchfield R, Hehre WJ, Pople JA (1971) Self-consistent molecular-orbital methods. ix. an extended Gaussian-type basis for molecular-orbital studies of organic molecules. J Chem Phys 54(2):724–728. https://doi.org/10.1063/1.1674902
- Khoirunisa V, Rusydi F, Boli LSP, Puspitasari I, Rachmawati H, Dipojono HK (2021) The significance of long-range correction to the hydroperoxyl radical-scavenging reaction of trans-resveratrol

- and gnetin C. J Mol Model 27(2):49. https://doi.org/10.1007/s00894-021-04680-2
- Troche-Pesqueira E, Pérez-Juste I, Navarro-Vázquez A, Cid MM (2013) A β-cyclodextrin–resveratrol inclusion complex and the role of geometrical and electronic effects on its electronic induced circular dichroism. J Mol Model 19(5):10242–10250. https://doi.org/10.1039/C3RA41972J
- Raiol A, Pinheiro M, Belo E, da Cunha AR, Marinho AM, Silva SY, Silva SC, Andrade-Filho T, Gester R (2021) Experimental and theoretical spectroscopic characterization, NLO response, and reactivity of the pharmacological agent spilanthol and analogues. J Mol Struct 1227:129423. https://doi.org/10.1016/j.molstruc.2020. 129423
- Andrade-Filho T, Silva T, Belo E, Raiol A, de Oliveira RV, Marinho PS, Bitencourt HR, Marinho AM, da Cunha AR, Gester R (2021) Insights and modelling on the nonlinear optical response, reactivity, and structure of chalcones and dihydrochalcones. J Mol Model 27(6):131182. https://doi.org/10.1007/s00894-021-04809-3
- Raiol A, da Cunha AR, Manzoni V, Andrade-Filho T, Gester R (2021) Solvent enhancement and isomeric effects on the NLO properties of a photoinduced cis-trans azomethine chromophore: a sequential MC/QM study. J Mol Model 27(9):3101. https://doi.org/10.1007/s00894-021-04809-3
- 33. Misra R, Maragani R, Pathak B, Gautam P, Mobin SM (2015) Star shaped ferrocenyl substituted triphenylamines. J Mol Model 21(11):71046–71051. https://doi.org/10.1007/s00894-015-2834-1
- Okuno K, Shigeta Y, Kishi R, Miyasaka H, Nakano M (2012) Tuned CAM-B3LYP functional in the time-dependent density functional theory scheme for excitation energies and properties of diarylethene derivatives. J Mol Model 18(9):29–34. https://doi. org/10.1007/s00894-012-1501-3
- Jacquemin D, Perpète EA, Scuseria GE, Ciofini I, Adamo C (2008) TD-DFT performance for the visible absorption spectra of organic dyes: conventional versus long-range hybrids. J Mol Model 14(1):123–135
- 36. Miertuš S, Scrocco E, Tomasi J (1981) Electrostatic interaction of a solute with a continuum. a direct utilizaion of ab initio molecular potentials for the prevision of solvent effects. Chem Phys 55(1):117–129. https://doi.org/10.1016/0301-0104(81)85090-2
- Coutinho K, Canuto S, Zerner MC (2000) A Monte Carlo-quantum mechanics study of the solvatochromic shifts of the lowest transition of benzene. J Chem Phys 112(22):9874–9880. https://doi.org/ 10.1063/1.481624
- Rivelino R, Cabral BJC, Coutinho K, Canuto S (2005) Electronic polarization in liquid acetonitrile: a sequential Monte Carlo/quantum mechanics investigation. Chem Phys Lett 407(1):13–17. https://doi.org/10.1016/j.cplett.2005.03.049
- Allen M, Tildesley D (1987) Computer simulation of liquids, Oxford science publications
- Almeida KJ, Coutinho K, Almeida WB, Rocha WR, Canuto S (2001) A Monte Carlo–quantum mechanical study of the solvatochromism of pyrimidine in water and in carbon tetrachloride. Phys Chemist Chem Phys 3:1583–1587. https://doi.org/10.1039/B100374G
- da Cunha AR, Duarte EL, Lamy MT, Coutinho K (2014) Protonation/deprotonation process of Emodin in aqueous solution and pKa determination: UV/Visible spectrophotometric titration and quantum/molecular mechanics calculations. Chem Phys 440:69

  79. https://doi.org/10.1016/j.chemphys.2014.06.009
- Jorgensen WL, Maxwell DS, Tirado-Rives J (1996) Development and testing of the OPLS all-atom force field on conformational energetics and properties of organic liquids. J Am Chem Soc 118(45):11225–11236. https://doi.org/10.1021/ja9621760



- Dodda LS, de Vaca IC, Tirado-Rives J, Jorgensen WL (2017) LigParGen web server: an automatic OPLS-AA parameter generator for organic ligands. Nucleic Acids Res 45(W1):W331–W336. https://doi.org/10.1093/nar/gkx312
- Breneman CM, Wiberg KB (1990) Determining atom-centered monopoles from molecular electrostatic potentials. the need for high sampling density in formamide conformational analysis. J Comput Chem 11(3):361–373. https://doi.org/10.1002/jcc. 540110311
- Berendsen HJC, Postma JPM, van Gunsteren WF, Hermans J (1981) Interaction models for water in relation to protein hydration. Reidel
- Lorentz HA (1880) Ueber die beziehung zwischen der fortpflanzungsgeschwindigkeit des lichtes und der körperdichte. Annalen der Physik 245:641–665. https://doi.org/10.1002/andp. 18802450406
- Lorenz L (1880) Ueber die refractionsconstante. Annalen der Physik 247:70–103. https://doi.org/10.1002/andp.18802470905
- Andrews DL, Thirunamachandran T (1979) Hyper-Raman scattering by chiral molecules. J Chem Phys 70(2):1027. https://doi.org/ 10.1063/1.437535
- Clays K, Persoons A (1991) Hyper-Rayleigh scattering in solution. Am Phys Soc 66(23):2980–2983. https://doi.org/10.1103/physrevlett.66.2980
- Gester R, Torres A, da Cunha AR, Andrade-Filho T, Manzoni V (2021) Theoretical study of thieno[3,4-b]pyrazine derivatives with enhanced NLO response. Chem Phys Lett 781:138976. https://doi.org/10.1016/j.cplett.2021.138976
- Muhammad S (2015) Second-order nonlinear optical properties of dithienophenazine and ttf derivatives: A butterfly effect of dimalononitrile substitutions. J Mol Graph Model 59:14–20. https://doi.org/10.1016/j.jmgm.2015.03.003
- Jaramillo P, Domingo LR, Chamorro E, Pérez P (2008) A further exploration of a nucleophilicity index based on the gas-phase ionization potentials. J Mol Struct: THEOCHEM 865(1):68–72. https://doi.org/10.1016/j.theochem.2008.06.022
- Barbosa-Silva R, Silva-Neto ML, Bain D, Modesto-Costa L, Andrade-Filho T, Manzoni V, Patra A, Araújo CB (2020) Observation and analysis of incoherent second-harmonic generation in gold nanoclusters with six atoms. J Phys Chem C 124(28):15440– 15447. https://doi.org/10.1021/acs.jpcc.0c03397
- Hazarika R, Kalita B (2021) Elucidating the therapeutic activity of selective curcumin analogues: DFT-based reactivity analysis. Struct Chem 32:1701–1715. https://doi.org/10.1007/s11224-021-01745-7
- 55. Frisch MJ, Trucks GW, Schlegel HB, Scuseria GE, Robb MA, Cheeseman JR, Scalmani G, Barone V, Petersson GA, Nakatsuji H, Li X, Caricato M, Marenich A, Bloino J, Janesko BG, Gomperts R, Mennucci B, Hratchian HP, Ortiz JV, Izmaylov AF, Sonnenberg JL, Williams-Young D, Ding F, Lipparini F, Egidi F, Goings J, Peng B, Petrone A, Henderson T, Ranasinghe D, Zakrzewski VG, Gao J, Rega N, Zheng G, Liang W, Hada M, Ehara M, Toyota K, Fukuda R, Hasegawa J, Ishida M, Nakajima T, Honda Y, Kitao O, Nakai H, Vreven T, Throssell K, Montgomery JA, Jr., Peralta JE, Ogliaro F, Bearpark M, Heyd JJ, Brothers E, Kudin KN, Staroverov VN, Keith T, Kobayashi R, Normand J, Raghavachari K, Rendell A, Burant JC, Iyengar SS, Tomasi J, Cossi M, Millam JM, Klene M, Adamo C, Cammi R, Ochterski JW, Martin RL, Morokuma K, Farkas O, Foresman JB, Fox DJ (2016) Gaussian 09, Revision A.02, gaussian Inc. Wallingford CT
- Lu T, Chen F (2011) Multiwfn: a multifunctional wavefunction analyzer. Wiley 33(5):580–592. https://doi.org/10.1002/jcc.22885
- Caruso F, Tanski J, Villegas-Estrada A, Rossi M (2004) Structural basis for antioxidant activity of trans-resveratrol: ab initio calculations and crystal and molecular structure. J Agric Food Chem 52(24):7279–7285. https://doi.org/10.1021/jf048794e

- Mikulski D, Molski M (2012) Quantum-mechanical computations on the electronic structure of trans-resveratrol and transpiceatannol: a theoretical study of the stacking interactions in trans-resveratrol dimers. J Mol Model 18(7):3255–3266. https:// doi.org/10.1007/s00894-011-1342-7
- Allan KE, Lenehan CE, Ellis AV (2009) UV light stability of α-cyclodextrin/resveratrol host-guest complexes and isomer stability at varying pH. Aust J Chem 62(8):921. https://doi.org/10.1071/ch08506
- Réka-Anita D, Chis V (2018) Conformational space and electronic absorption properties of the two isomers of resveratrol. Studia Universitatis Babeş-Bolyai Physica 62. https://doi.org/10.24193/ subbphys.2017.05
- Allan KE, Lenehan CE, Ellis AV (2009) UV light stability of
  -cyclodextrin/resveratrol hostguest complexes and isomer stability at varying pH. Aust J Chem 62(8):921–926. https://doi.org/10.
  1071/CH08506
- Figueiras TS, Neves-Petersen MT, Petersen SB (2011) Activation energy of light induced isomerization of resveratrol. J Fluoresc 21(5):1897–1906. https://doi.org/10.1007/s10895-011-0886-3
- Pavone FS, Campagnola PJ (eds) (2016) Second harmonic generation imaging, CRC Press. Ch. 4:81–102. https://doi.org/10.1201/ h15039
- Pimenta ACM, Andrade-Filho T, Manzoni V, Nero JD,Gester R (2019) Giant values obtained for first hyperpolarizabilities of methyl orange: a DFT investigation. Theor Chem Accounts 138(2). https://doi.org/10.1007/s00214-018-2406-x
- Andrade-Filho T, Silva T, Belo E, Raiol A, de Oliveira RV, Marinho PS, Bitencourt HR, Marinho AMR, da Cunha AR, Gester R (2021) Insights and modelling on the nonlinear optical response, reactivity, and structure of chalcones and dihydrochalcones. J Mol Struct 1246:131182. https://doi.org/10.1016/j.molstruc.2021.131182
- Oudar JL, Chemla DS (1977) Hyperpolarizabilities of the nitroanilines and their relations to the excited state dipole moment. J Chem Phys 66(6):2664–2668. https://doi.org/10.1063/1.434213
- Zyss J (1979) Hyperpolarizabilities of substituted conjugated molecules. III. study of a family of donor–acceptor disubstituted phenyl-polyenes. J Chem Phys 71(2):909–916. https://doi.org/10. 1063/1.438380
- 68. Cheminet N, Nogueira SL, Benaqqa O, Malki ZE, Bourass M, Cassegrain S, Hamidi M, Bouachrine M, Sotiropoulos JM, Miqueu K, Jarrosson T, Niebel C, Lère-Porte JP, Serein-Spirau F (2020) Elaboration of low-band-gap π-conjugated systems based on thieno[3,4-b]pyrazines. Pure Appl Chem 92(2):335–353. https://doi.org/10.1515/pac-2018-1009
- 69. Alam MJ, Khan AU, Alam M, Ahmad S (2019) Spectroscopic (FTIR, FT-RAMAN, <sup>1</sup>H NMR and UV-vis) and DFT/TD-DFT studies on cholesteno [4,6-b, c]-2',5'-dihydro-1',5'-benzothiazepine. J Mol Struct 1178:570–582. https://doi.org/10.1016/j.molstruc.2018.10.063
- Muhammad S, Shehzad RA, Iqbal J, Al-Sehemi AG, Saravanabhavan M, Khalid M (2019) Benchmark study of the linear and nonlinear optical polarizabilities in proto-type NLO molecule of para-nitroaniline. J Theo Comput Chem 18(06):1950030. https://doi.org/10.1142/S0219633619500305
- Chandrakumar KRS, Ghanty TK, Ghosh SK (2004) Relationship between ionization potential, polarizability, and softness: a case study of lithium and sodium metal clusters. J Phys Chem A 108(32):6661–6666. https://doi.org/10.1021/jp048522e
- Gupta K, Ghanty TK, Ghosh SK (2012) Polarizability, ionization potential, and softness of water and methanol clusters: an interrelation. J Phys Chem A 116(25):6831–6836. https://doi.org/10.1021/ jp3048357
- Scott Obach R, Kalgutkar A (2010) Reactive electrophiles and metabolic activation, Oxford, pp 309–347. https://doi.org/10.1016/ B978-0-08-046884-6.00115-9



 Domingo LR, Aurell MJ, P P, Contreras R (2002) Quantitative characterization of the global electrophilicity power of common diene/dienophile pairs in Diels–Alder reactions. Tetrahedron 58(22):4417–4423. https://doi.org/10.1016/S0040-4020(02)00410-6 **Publisher's Note** Springer Nature remains neutral with regard to jurisdictional claims in published maps and institutional affiliations.

Springer Nature or its licensor (e.g. a society or other partner) holds exclusive rights to this article under a publishing agreement with the author(s) or other rightsholder(s); author self-archiving of the accepted manuscript version of this article is solely governed by the terms of such publishing agreement and applicable law.

# **Authors and Affiliations**

Igo T. Lima<sup>1</sup> · Ramon F. C. Gomes<sup>1</sup> · Edson N. C. Paura<sup>2</sup> · Patricio F. Provasi<sup>3</sup> · Rodrigo Gester<sup>4,5</sup> · Antonio Rodrigues da Cunha<sup>2</sup>

- Antonio Rodrigues da Cunha cunha.antonio@ufma.br
- Coordenação do Bacharelado Interdisciplinar em Ciência e Tecnologia, Campus Dom Delgado, Universidade Federal do Maranhão, UFMA, São Luís, MA, Brazil
- Universidade Federal do Maranhão, UFMA, Campus Balsas, Balsas, MA, Brazil
- Department of Physics, IMIT, Northeastern University, CONICET, AV. Libertad 5500, W 3404 AAS, Corrientes, Argentina
- Faculdade de Física, Universidade Federal do Sul e Sudeste do Pará, UNIFESSPA, Marabá, PA, Brazil
- Instituto de Física, Universidade de São Paulo, USP, Rua do Matão 1371, São Paulo, SP, Brazil

